Convective craton self-compression and its role for stabilization of old lithosphere

=list all authors here=

$^{=number=}$=Affiliation Address=

Key Points:

- Cratons self-induce compressive tractions along their periphery
- Compression arises due to the diversion of mantle flow in presence of thick and viscous cratons
- Such compressive tractions could help in stabilizing older lithosphere

Corresponding author: =name=, `=email address=`

Abstract

The density and viscosity of thick cratonic roots are key for their stability. Despite being exposed to convective stresses for long times, continental roots appear capable of resisting mantle shearing. This can be attributed to their higher strength, i.e., viscosity. But such high viscosity also leads to higher tractions along their edges and more efficient force transmission compared to other parts of the lithosphere. We develop numerical models to further investigate the origin of these high tractions surrounding cratons and examine if they have any contribution towards the long-term survival of cratons. Our results show that due to thick and viscous cratonic roots, mantle flow can be diverted along the periphery of cratons. Hence, the horizontal gradient of vertical velocity changes at the craton periphery. Even a small change in the velocity gradient multiplied with the large viscosity can produce high tractions in these regions. Additionally, the resultant vector of the vertical velocity gradient becomes convergent along the craton margin, which eventually controls the direction of traction around cratons. Such convergent tractions could probably serve to stabilize cratons against mantle shearing by adding an additional factor in cratons' longevity.

Plain Language Summary

Cratons are the oldest continental relicts on Earth. Due to Earth's plate tectonics and mantle convection, many non-cratonic rocks get recycled. However, cratons have escaped the tectonic recycling, and some remained stable for more than ~ 3 billion years. How cratons have survived for such a long time has remained elusive. Previous studies have shown that the high strength and neutral buoyancy of cratons provide them with a tectonic stability. In this study, we show that self-induced compression along the edges of cratons may further help them to resist tectonic recycling.

1 Introduction

Cratons are relics of the oldest continental lithosphere, surviving since the Archean (Pearson & Wittig, 2014; Pearson et al., 1995; Pearson, 1999). Structurally, cratons have thick lithospheric roots, or cratonic keels (Gung et al., 2003; Polet & Anderson, 1995), that are likely cold because they are characterized by fast seismic velocities (Auer et al., 2014; Ritsema et al., 2011; Simmons et al., 2010). Low measured heat fluxes of cratonic lithosphere reaffirm the argument for colder cratons (Rudnick et al., 1998). The endurance of Archean cratons against Earth's tectonic and convective recycling is highly debated (cf. Yoshida & Yoshizawa, 2021), but proposed reasons for cratonic stability draw from geochemical and geophysical perspectives (Jordan, 1975, 1978; King, 2005; Lenardic & Moresi, 1999; Lenardic et al., 2000, 2003; Paul et al., 2019; Paul & Ghosh, 2020; Sleep, 2003; O'Neill et al., 2008; Wang et al., 2014; Yoshida, 2010, 2012). One of the oldest hypotheses proposed that cratons are constituted of chemically lighter elements that help them to float above the convective mantle without sinking into it (Jordan, 1975, 1978). However, subsequent numerical models showed that chemical buoyancy alone cannot protect cratons from the continuous convective shearing exerted by the mantle flow. Instead, root thickness and viscosity are the two prime factors that can resist deformation against mantle shearing (Lenardic & Moresi, 1999; Lenardic et al., 2003; O'Neill et al., 2008; Paul et al., 2019; Paul & Ghosh, 2020; Sleep, 2003).

To understand the role of craton viscosity, previous studies quantified the nature of tractions exerted by mantle flow at the base of the lithosphere, and the strain-rates associated with deformation there (Conrad & Lithgow-Bertelloni, 2006; Cooper & Conrad, 2009; Naliboff et al., 2009; Paul et al., 2019). Conrad & Lithgow-Bertelloni (2006) showed that tractions increase as the lithospheric thickness increases. Paul et al. (2019) found a similar amplification of tractions, but also showed that the strain-rates at the cratonic base diminish as lithospheric roots get thicker. This inverse relation between

tractions and the strain-rates may slow the deformation of a cratonic root, and therefore might be an important factor for the long-term survival of cratons. Cooper & Conrad (2009) attributed elevated tractions at the base of cratons to greater coupling to mantle flow, which has been noted in models with thick cratonic roots (Zhong, 2001; Becker, 2006). However, more recent models, especially those employing free-slip surface boundary conditions that more closely resemble earth's own conditions, show that tractions are primarily amplified along the periphery of cratons (fig. 3 from Paul et al., 2019). Although Paul et al. (2019) speculated that cratonic edges might more effectively absorb mantle stresses compared to cratonic interiors, a proper quantitative analysis of such a phenomenon is lacking.

Here, we explore the origin of higher tractions along craton boundaries and consider their implications on the stability of cratons. We develop instantaneous spherical numerical models of mantle convection and examine how mantle flow is modified due to the presence of thick and viscous cratons. We hypothesize that cratons' high viscosity roots can divert mantle flow, which may induce higher traction at the craton periphery. We test our hypothesis using various models having different viscosities for cratons, asthenosphere and non-cratonic lithosphere. Finally, we consider how such high tractions generated by the cratons themselves may support cratonic stability against mantle shearing, and therefore could be essential to cratonic longevity.

2 Mantle convection models

We use the finite element code CitcomS to develop instantaneous spherical models of mantle convection (Zhong et al., 2000). The code assumes the mantle to be a viscous and incompressible fluid. It solves the conservation of mass, momentum, and energy equations with the Boussinesq approximation and infinite Prandtl number. The smallest resolution of our models in the horizontal direction is $\sim 0.7^o \times 0.7^o$. The vertical resolution in the top 300 km is 24 km, and from 300 km to CMB it is ~ 50 km. Mantle flow is driven by the density anomalies obtained from SMEAN2 seismic tomography, which is a combination of S40RTS (Ritsema et al., 2011), GyPSuM-S (Simmons et al., 2010) and SAVANI (Auer et al., 2014) models. A velocity-density scaling value of 0.25 is used to convert velocity anomalies into density anomalies (cf. Paul et al., 2019). Higher velocity regions under the continents were removed till 300 km to impose neutrally buoyant cratons (cf. Paul et al., 2019). We keep a free-slip boundary condition at the surface and at the core-mantle boundary. Reference viscosity, Rayleigh number, thermal expansivity and the thermal conductivity values are kept at 10^{21} Pa.s, $4{\times}10^8$, $3{\times}10^{-1}K^{-1}$, and $10^{-6}m^2/s$ respectively.

In our models, the mantle is divided into four layers based on their relative viscosity w.r.t. to the upper mantle (300-600 km) reference viscosity, which we consider to be 10^{21} Pa.s. The top 100 km is assigned as the lithosphere, which is 30× more viscous than the reference mantle viscosity. Asthenosphere (100-300 km) is made 10x weaker than the reference mantle, having a relative viscosity of 0.1, and the lower mantle (660-2900 km) is made 50× stronger than the reference mantle. On top of this radially-varying viscosity structure, we impose lateral viscosity variations. We approximate temperature-dependent viscosity using a linearised Arrhenius law $\eta = \eta_0 \times \exp(E(T_0 - T))$, where η_0 is the radial viscosity of any layer, T_0 is the non-dimensionalised reference temperature, and T is the non-dimensionalised actual temperature. In our models, the reference temperature T_0 is set to 0.5, and the range of non-dimensional temperature varies from 0 - 1, where the maximum temperature (1) is 1300^o C. E is a dimensionless number that controls the strength of temperature dependence. We have tested several models to find the suitable values of E (cf. Paul et al., 2019) and keep it to 5. Temperature-dependent viscosity produces 10x weak plate margins compared to the continental interiors. We also incorporate high viscosity cratons in our models, where the locations of cratons are taken from the 3SMAC model (Nataf & Ricard, 1996). Cratons are made 10×, 100×, and 1000×

more viscous than the surrounding lithosphere, and they have uniformly viscous keels up to a depth of 300 km (Paul et al., 2019). We have also varied the relative viscosity of asthenosphere to 0.01 (10^{19} Pa.s) and 1 (10^{21} Pa.s) to test the consistency of our results with respect to the radial viscosity structure of the mantle. In one of the cases, we have made lithosphere highly viscous with a relative viscosity 150 times the reference value. Our reference models omit cratons and only incorporates temperature-dependent viscosity to create lateral viscosity variations.

3 Tractions within cratons

We analyse the $r\phi$ and $r\theta$ components of stress tensor from our model outputs and calculate traction vectors (τ_0) from the reference model (Fig. 1). In the reference model, the magnitude of traction vectors are restricted within ~ 5 MPa, and their orientation are guided by density anomalies imposed in the model (Fig. 1 a). Incorporating cratons in the model change the traction vectors (τ) become convergent along the edge of cratons (Fig. 1b). A few zoomed in maps near the cratonic regions show this effect more prominently (Figs. 1 c-f). The South American cratons show the most significant pattern of convergent tractions along their periphery (Fig. 1 c). North American, Scandinavian and the South African cratons are relatively bigger in size, and the large tractions can only be seen within the peripheral part, leaving the craton core (Figs. 1d-f). Smaller cratons like Australia and India also show similar convergent tractions (Figs. 1 g,h). Across all cratons such convergent traction can attribute a compressive regime within them.

Apart from the change in direction, magnitude of traction vectors have also increased notably. To quantify the increment of traction magnitude, we normalize the traction magnitude from models with craton to the reference model ($|\tau|/|\tau_0|$). Hence, the traction ratio for the reference model is always 1. In the presence of cratons that are $100\times$ more viscous than the rest of the lithosphere, the maximum traction ratio increases by up to $80\times$ to $100\times$ at ~ 120 km depth along the edge of cratons (Fig. 1 c-f). The magnitude of the traction ratio along the craton edges can be influenced by the viscosity structure imposed in our models (Fig. 2). To investigate the dependence of viscosity structure and depth on the traction ratio, we calculate the average traction ratio at various depths along the edges of cratons (Fig. 2 a). Edge of the cratons is identified by the regions having traction ratio more than 5. The general trend shows that the average traction ratio is close to 15 within the top 100 km of cratons, where they are surrounded by viscous lithosphere. The average traction ratios then increase with depth, reaching their peak values in the mid-craton depth range ~ 160 km. Highest traction ratio at this depth could possibly occur as the horizontal velocity reaches the peak velocity in the mid-asthenosphere depth. Proceeding deeper, the traction ratio gradually falls before reaching another peak near the base of cratons at ~ 270 km depth. The exact magnitude of the traction ratio depends on the combination of craton and asthenosphere viscosity. Highly viscous ($1000\times$) cratons exhibit the largest maximum traction ratios, which reach their peak of 30-35 in the mid-asthenospheric depth region. Models with smaller viscosity contrasts (e.g., stronger asthenosphere with relative viscosity 1) exhibit relatively smaller tractions at the craton edges, whereas weaker asthenosphere (relative viscosity 0.1, 0.01) is consistent with larger tractions. We have tested a model with high lithospheric viscosity ($150\times$), and similarly found large traction ratios along cratons' periphery, except in the top 100 km, where the highly viscous lithosphere exerts large tractions at the craton boundary.

4 Origin of compression along craton periphery

Our models demonstrate a change of traction to a highly compressive state in the presence of viscous cratons. However, the origin of such a regional compressive regime

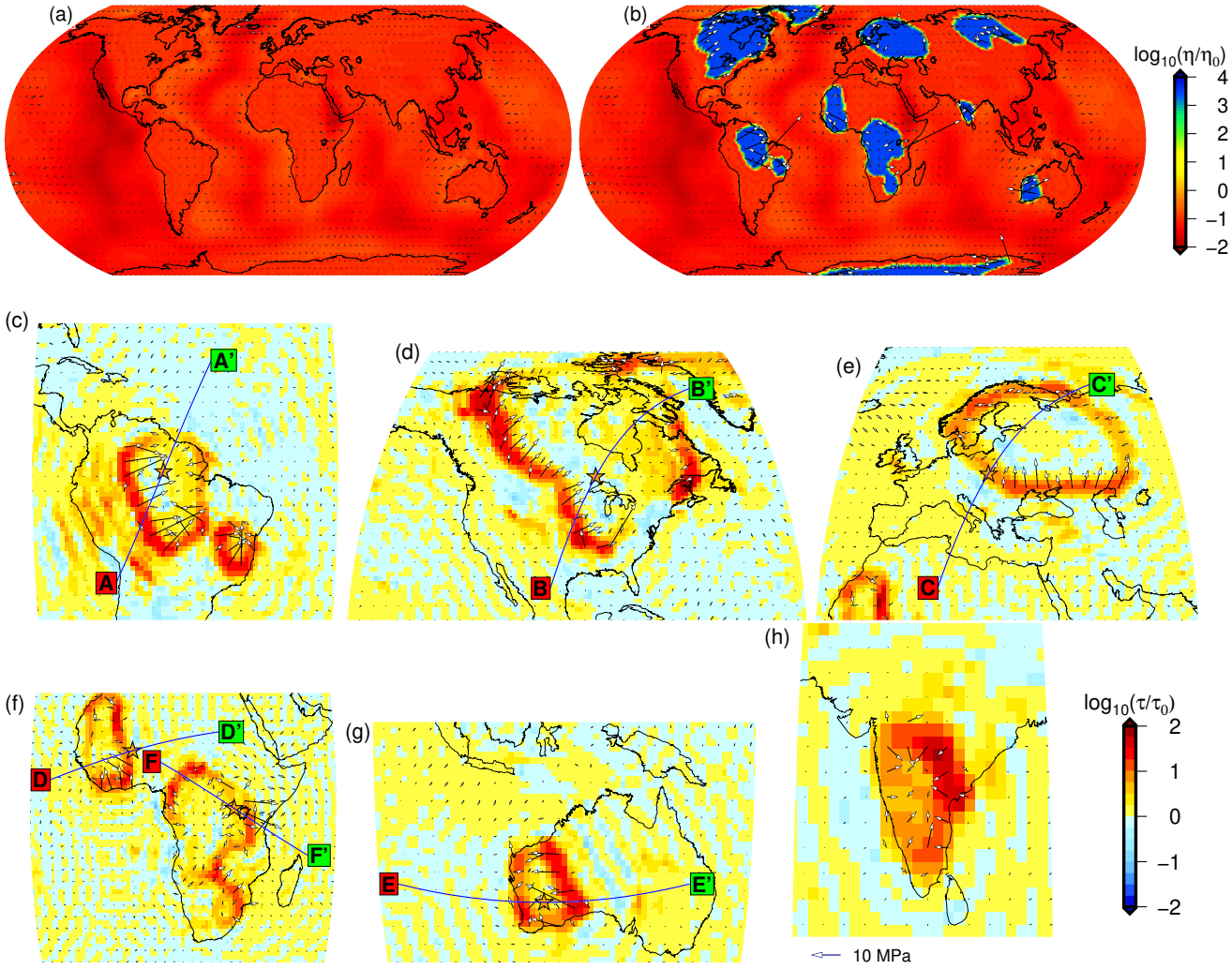

Figure 1. Global traction patterns in the absence and presence of cratons at 120 km depth. (a) Traction in reference model without cratons, (b) Traction in model with 0.1 relative viscosity of asthenosphere and cratons that are 100× more viscous than the surrounding lithosphere. Background colors indicate viscosity and arrows represent the magnitude and direction of absolute traction. (c)-(h) Zoomed in traction plots near cratonic regions of South America (c), North America (d), Scandinavia (e), Africa(f), Australia (g) and India (h). The background colors represent logarithm of traction ratio. Velcotiy cross-sections along the six transects (AA' - FF') are shown in Fig. 4

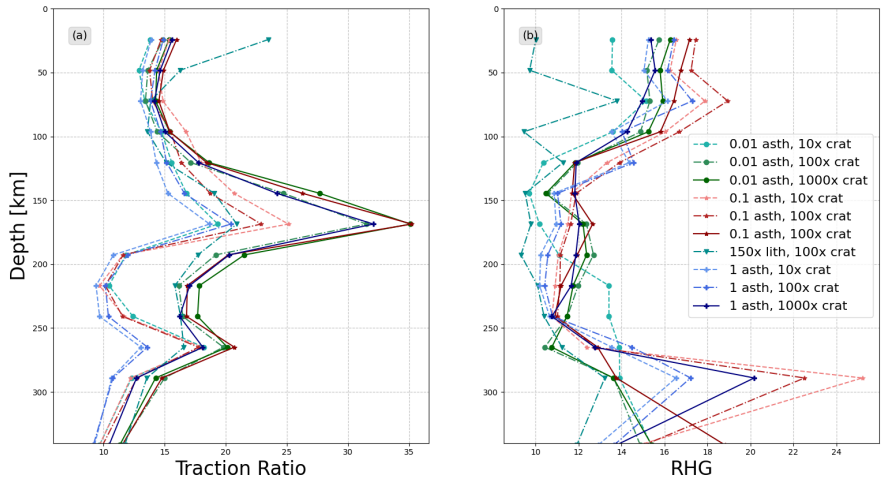

Figure 2. (a) Depth variation of the average traction ratio along the craton periphery from different models. (b) Depth variation of ratio of horizontal velocity gradient (RHG) along the craton periphery from different models. A description of the different models is given in the index.

in the presence of thick and viscous cratons needs to be investigated. Traction vector is calculated from σ_{xz} and σ_{yz} components, where

$$\sigma_{xz} = \eta(\frac{\partial u}{\partial z} + \frac{\partial \omega}{\partial x}) \tag{1}$$

$$\sigma_{yz} = \eta(\frac{\partial v}{\partial z} + \frac{\partial \omega}{\partial y}) \tag{2}$$

u, v, and ω are the horizontal and vertical components of the velocity vector and η is the viscosity. The magnitude of traction is given by,

$$|\tau| = \eta\sqrt{(\frac{\partial u}{\partial z} + \frac{\partial \omega}{\partial x})^2 + (\frac{\partial v}{\partial z} + \frac{\partial \omega}{\partial y})^2} \tag{3}$$

Conceptually, the presence of a thick and highly viscous craton can obstruct asthenospheric flow in horizontal direction, and can possibly deflect it downward. Such velocity diversion can make the u and v components extremely small near the craton edge, implying that the first terms in equations 1 and 2 will be negligible. However, if the downward diversion is strong, the vertical velocity (ω) component along the horizontal direction increases gradually towards cratons. Hence, the horizontal gradient of the vertical velocity components, i.e., the second term in the equation 1 and 2 become the controlling factor for the origin of high tractions along craton boundaries. We test this hypothesis by calculating the horizontal gradient of vertical velocities as:

$$\nabla^{\mathrm{v}}_{\mathrm{h}} = \sqrt{(\frac{\partial \omega}{\partial \mathrm{x}})^2 + (\frac{\partial \omega}{\partial \mathrm{y}})^2} \tag{4}$$

To analyze the effect of thick cratons in changing the gradient, we take the ratio of the horizontal velocity gradient (RHG) as:

$$\mathrm{RHG} = \frac{(\nabla^{\mathrm{v}}_{\mathrm{h}})_{\mathrm{craton}}}{(\nabla^{\mathrm{v}}_{\mathrm{h}})_{\mathrm{no\_craton}}} \tag{5}$$

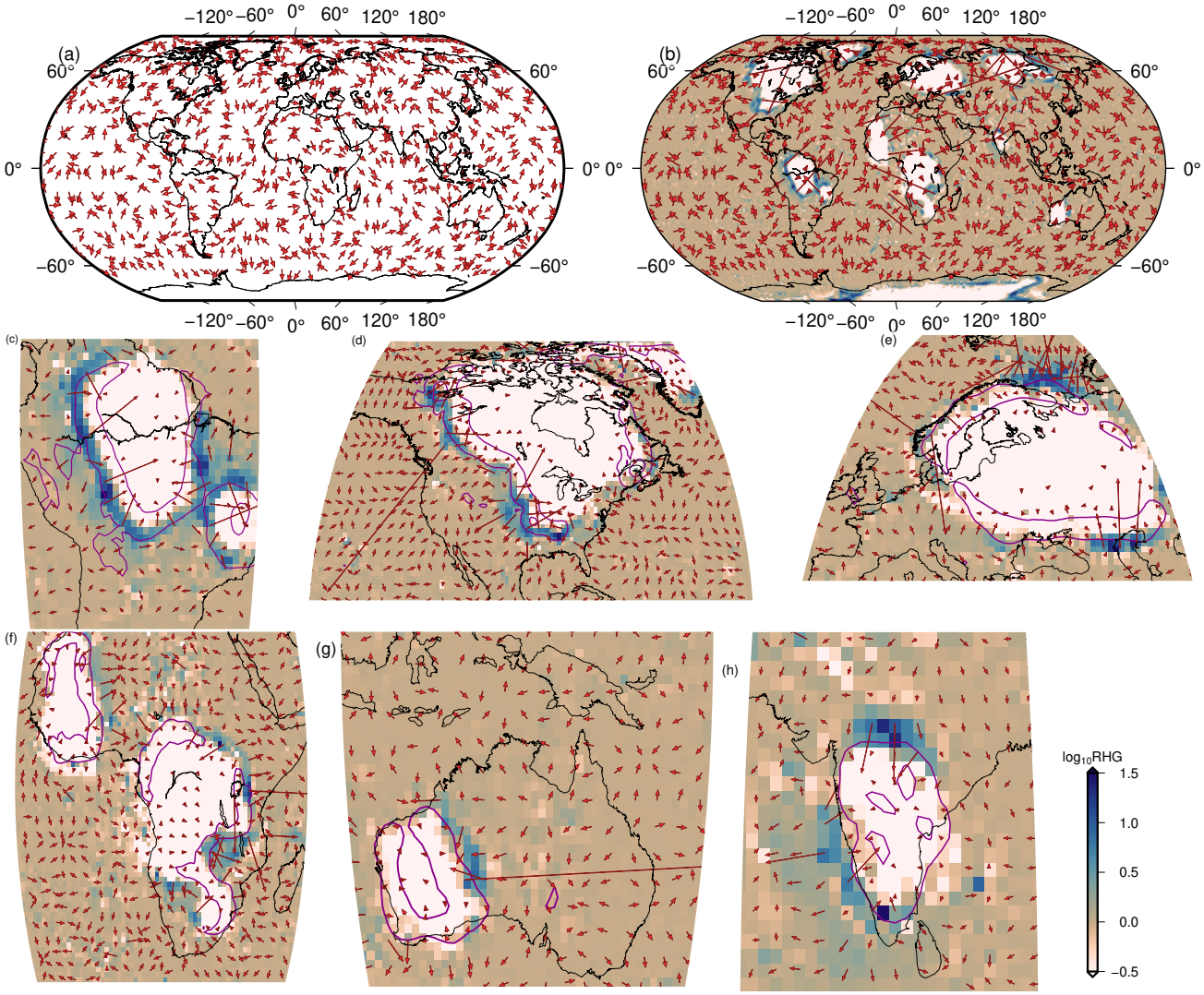

Figure 3. Ratio of horizontal velocity gradients of vertical velocity vectors (RHG) from different models at 120 km depth.(a) RHG vectors in reference model. (b) RHG vectors in the model with 0.1 relative viscosity of asthenosphere and cratons that are 100× more viscous than the surrounding lithosphere. Background colors represent magnitude of RHG. Magnitude of vectors are exactly the same as the color. (c)-(h) Zoomed-in plots of RGH near cratonic regions. Violet lines encircle areas where the traction ratio (shown in Fig. 1 b) is greater than 5.

RHG can quantify the concentration of downward flow due to the presence of viscous cratons, where RHG >> 1 indicates stronger vertical velocity deflection. We also calculate the vector direction of the horizontal velocity gradients as $tan^{-1}(\frac{\partial\omega}{\partial y}/\frac{\partial\omega}{\partial x})$. For the reference model, there is no change of vector direction near craton margin (Fig. 3a), however, vectors change their direction in presence of cratons (Fig. 3b). Additionally, there are rings of high value of RHG along the craton periphery (Fig. 3b). Within the periphery of The South American craton, RHG vectors most prominently show convergent patterns similar to tractions (Fig. 3c). Other cratons also produce convergent RHG vectors along their periphery along with high value of RHG upto 20-30× (Figs. 3d-h). Contours of traction ratio greater than 5 are plotted to visualise the coherence of RHG and zones of high traction on the craton edges. High RHG values can be interpreted as the vertical velocity is increasing near the craton boundary, which is possible if cratons can self-induce downwelling flows along their periphery. We investigate how this downwelling varies with the depth and viscosity structures in our models. We consider areas of high RHG values (≥ 5) which occur along craton periphery, and calculate their average values (Fig. 2b). In the top 100 km, the average RHG varies within 15-17, except for the 150 viscous lithosphere case. In the mid-cratonic depth range (100-250 km), the average RHG value decreases slightly and varies within 10-13. Beyond 250 km depth, RHG increases again reaching a peak occurs near the base of cratons, likely because of the concentrated flow below them.

We compare the velocity cross-sections from our models with and without cratons to investigate the nature of flow velocity diversion along cratons. Cross-sections underneath the South American and the North American cratons show notable changes in velocity along their western margin. In both cases, the mantle flows from west to east in absence of cratons due to density differences imposed in our models (Figs. 4a, b). Convergent flow in the west of the South American craton occurs due to a subducting slab. In the presence of a thick and viscous craton, the convergent flow velocity is now diverted along the craton margin and gets concentrated below it (Fig. 4 a). Similar velocity diversion is also visible around the western margin of the North American craton, where the flow gets diverted downwards and concentrated below the craton (Fig. 4 b). Scandinavian craton show weak velocity diversion, and hence the amplitude of convergent traction is also low in this craton (Fig. 4 c). Size of the Western African craton is significantly smaller than the rest, but the change of velocity field is much pronounced. A downward flow along the Eastern margin of the craton is a clear indicative of change in RHG (Fig. 4 d). Australian craton also show a small velocity diversion (Fig. 4 e). Due to the smaller size of cratons (e.g., Indian craton), diversion of velocity vectors may not be visible clearly. Nevertheless, tractions are the results of velocity gradient multiplied with viscosity (see equation 3). Viscosity being a very large number (in the order of 10^{21}), a very small change of velocity gradient can produce a sharp change in the traction magnitude and direction. One significant change is observed for the South African craton where the mantle is flowing upward (Fig. 4f). Even in this case, the horizontal velocities get diminished due to the craton and vertical velocities become stronger along the craton boundary. Hence, despite within a zone of divergent velocities (Conrad et al., 2013), tractions along the South Afican craton margin remain convergent.

5 Implications for craton stabilization

We find that the stiffness of cratons causes them to self-induce a convergent traction along their periphery. The magnitude of these tractions depends on the viscosity structure of craton, asthenosphere and lithosphere. In presence of a 100× viscous craton, traction magnitude goes up to 15-20 MPa (Figs. 1b-h) which is 25-30 × larger than the case without presence of cratons. The inward-directed orientation of tractions along the craton boundary appears to be a universal phenomenon (Figs. 1b). We infer that such convergent tractions originate from the diversion of mantle flow velocity due to the

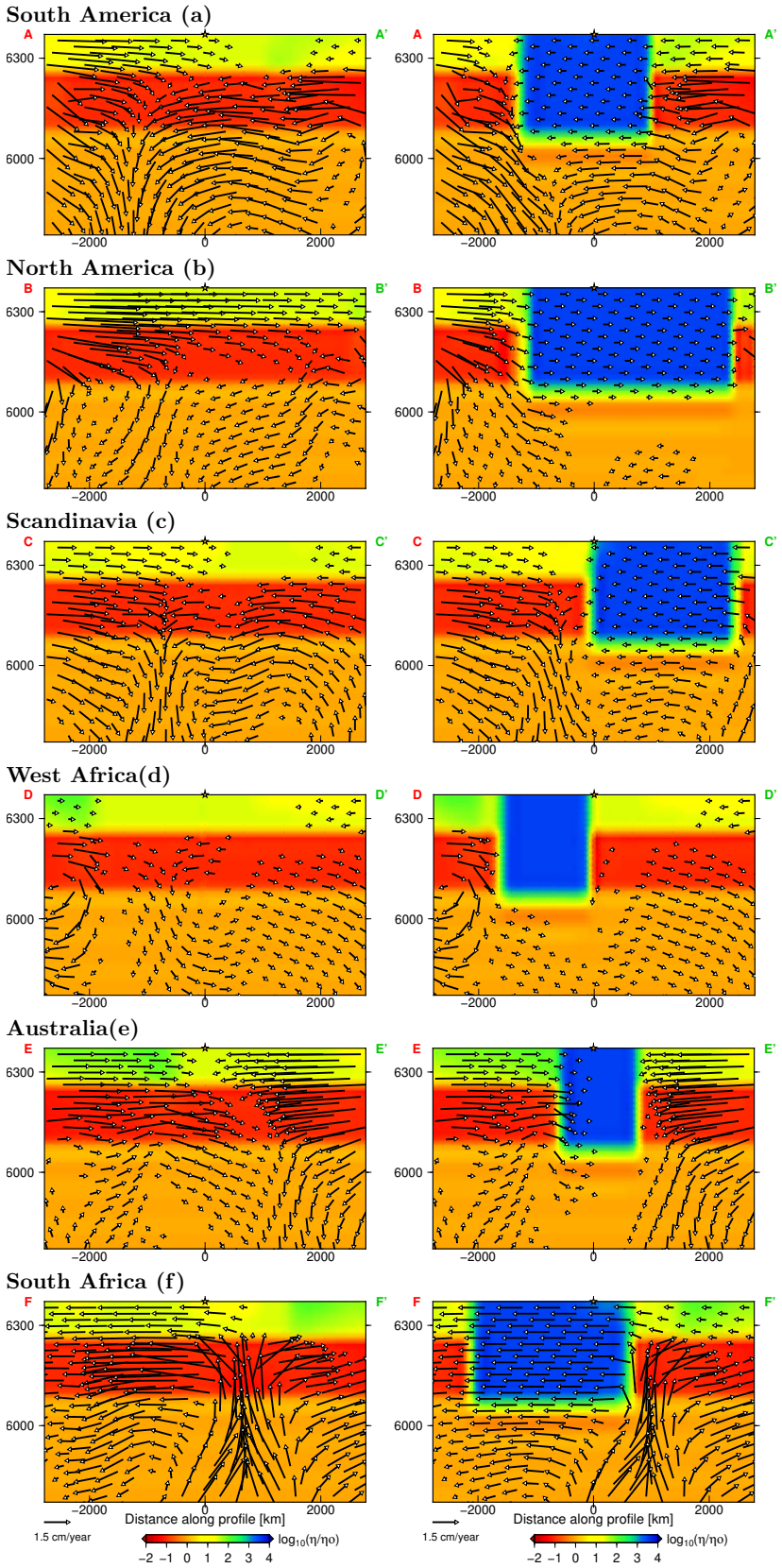

Figure 4. Velocity cross-sections under cratons along the transects shown in Fig. 1c-g. Background colors represents logarithm of relative viscosity, and the arrows represent velocity vectors along the transect.

thick and viscous cratonic roots. We test our hypothesis by calculating the ratio of horizontal gradient of vertical velocity (RHG, equation 5). Our calculations indicates that the mantle flow starts downwelling along craton margins and the this velocity gradient controls the state of traction along the craton periphery. In case of African craton, where the flow velocity is strongly upwelling, presence of a strong craton can also affect the vertical velocities. By definition, tractions are the outcome of velocity gradient multiplied by viscosity, a slight change of velocity gradient can cause drastic change in tractions. Due to change in vertical velocity along the craton margins, they experience compressive tractions. We also calculate the vectors associated with the RHG and show that they also become convergent along the craton margin. Hence, we infer that the change of vertical velocity in the horizontal direction is the key to strong convergent tractions along craton boundary.

Previous studies have attributed the long-term stability of cratons to their thickness, viscosity and chemical buoyancy (Lenardic et al., 2003; Paul et al., 2019). We suggest that self-induced compressive tractions along craton boundaries could be another critical factor that has made cratons stable across billions of years. During the formation of cratons, it is likely that they were located in a compressed ste up to become thicker (Beall et al., 2018; Capitanio et al., 2020; Wang et al., 2018). However, the mechanism of such compression has remained controversial. It could be possible that juvenile viscous cratonic roots deflected the horizontal velocity in vertical directions and thus self-induced compressional tractions along the their periphery. These compressive tractions could help cratonic longevity in two ways. Primarily, they can hold the craton tightly against the convective shearing of the mantle. Additionally, compressive tractions in turn could help in the gradual thickening of the cratonic roots over billion years, which became a key factor for cratonic survival.

Acknowledgments

All models were developed in Cray XC40 system at the Supercomputer Education and Research Centre (SERC), IISc. This work was supported by the Norwegian Research Council projects 223272 (Centre of Excellence) and 288449 (MAGPIE Project).

References

Auer, L., Boschi, L., Becker, T., Nissen-Meyer, T., & Giardini, D. (2014). Savani: A variable resolution whole-mantle model of anisotropic shear velocity variations based on multiple data sets. *Journal of Geophysical Research: Solid Earth*, *119*(4), 3006–3034.

Beall, A., Moresi, L., & Cooper, C. (2018). Formation of cratonic lithosphere during the initiation of plate tectonics. *Geology*, *46*(6), 487–490.

Becker, T. W. (2006). On the effect of temperature and strain-rate dependent viscosity on global mantle flow, net rotation, and plate-driving forces. *Geophysical Journal International*, *167*(2), 943–957.

Capitanio, F. A., Nebel, O., & Cawood, P. A. (2020). Thermochemical lithosphere differentiation and the origin of cratonic mantle. *Nature*, *588*(7836), 89–94.

Conrad, C. P., & Lithgow-Bertelloni, C. (2006). Influence of continental roots and asthenosphere on plate-mantle coupling. *Geophysical Research Letters*, *33*, L05 312, doi:10.1029/2005GL025621.

Conrad, C. P., Steinberger, B., & Torsvik, T. H. (2013). Stability of active mantle upwelling revealed by net characteristics of plate tectonics. *Nature*, *498*(7455), 479–482.

Cooper, C., & Conrad, C. P. (2009). Does the mantle control the maximum thickness of cratons? *Lithosphere*, *1*(2), 67–72.

Gung, Y., Panning, M., & Romanowicz, B. (2003). Global anisotropy and the thickness of continents. *Nature*, *422*(6933), 707–711.

Jordan, T. (1975). The continental tectosphere. *Reviews of Geophysics*, *13*(3), 1–12.

Jordan, T. (1978). Composition and development of the continental tectosphere. *Nature*, *274*(5671), 544–548.

King, S. (2005). Archean cratons and mantle dynamics. *Earth and Planetary Science Letters*, *234*(1), 1–14.

Lenardic, A., & Moresi, L. N. (1999). Some thoughts on the stability of cratonic lithosphere: effects of buoyancy and viscosity. *Journal of Geophysical Research: Solid Earth*, *104*(B6), 12747–12758.

Lenardic, A., Moresi, L. N., & Mühlhaus, H. (2000). The role of mobile belts for the longevity of deep cratonic lithosphere: the crumple zone model. *Geophysical Research Letters*, *27*(8), 1235–1238.

Lenardic, A., Moresi, L. N., & Mühlhaus, H. (2003). Longevity and stability of cratonic lithosphere: insights from numerical simulations of coupled mantle convection and continental tectonics. *Journal of Geophysical Research: Solid Earth*, *108*(B6), https://doi.org/10.1029/2002JB001859.

Naliboff, J. B., Conrad, C. P., & Lithgow-Bertelloni, C. (2009). Modification of the lithospheric stress field by lateral variations in plate-mantle coupling. *Geophysical Research Letters*, *36*(22).

Nataf, H.-C., & Ricard, Y. (1996). 3SMAC: an a priori tomographic model of the upper mantle based on geophysical modeling. *Physics of the Earth and Planetary Interiors*, *95*(1-2), 101–122.

O'Neill, C., Lenardic, A., Griffin, W., & O'Reilly, S. (2008). Dynamics of cratons in an evolving mantle. *Lithos*, *102*(1), 12–24.

Paul, J., & Ghosh, A. (2020). Evolution of cratons through the ages: A time-dependent study. *Earth and Planetary Science Letters*, *531*, 115962,

https://doi.org/10.1016/j.epsl.2019.115962.

Paul, J., Ghosh, A., & Conrad, C. (2019). Traction and strain rate at the base of the lithosphere: An insight into cratonic stability. *Geophysical Journal International*, *217*(2), 1024–1033.

Pearson, D. (1999). The age of continental roots. *Lithos*, *48*(1), 171–194.

Pearson, D., Carlson, R., Shirey, S., Boyd, F., & Nixon, P. (1995). Stabilisation of Archaean lithospheric mantle: A Re-Os isotope study of peridotite xenoliths from the Kaapvaal craton. *Earth and Planetary Science Letters*, *134*(3), 341–357.

Pearson, D., & Wittig, N. (2014). The formation and evolution of cratonic mantle lithosphere–evidence from mantle xenoliths. In K. Turekian & H. Holland (Eds.), *In treatise on geochemistry* (p. 255-292). New York: Elsevier.

Polet, J., & Anderson, D. (1995). Depth extent of cratons as inferred from tomographic studies. *Geology*, *23*(3), 205–208.

Ritsema, J., Deuss, a. A., Van Heijst, H., & Woodhouse, J. (2011). S40rts: a degree-40 shear-velocity model for the mantle from new Rayleigh wave dispersion, teleseismic traveltime and normal-mode splitting function measurements. *Geophysical Journal International*, *184*(3), 1223–1236.

Rudnick, R., McDonough, W., & O'Connell, R. (1998). Thermal structure, thickness and composition of continental lithosphere. *Chemical Geology*, *145*(3), 395–411.

Simmons, N. A., Forte, A. M., Boschi, L., & Grand, S. P. (2010). Gypsum: A joint tomographic model of mantle density and seismic wave speeds. *Journal of Geophysical Research: Solid Earth*, *115*, https://doi.org/10.1029/2010JB007631.

Sleep, N. H. (2003). Survival of Archean cratonal lithosphere. *Journal of Geophysical Research: Solid Earth*, *108*(B6).

Wang, H., van Hunen, J., & Pearson, D. G. (2018). Making Archean cratonic roots by lateral compression: a two-stage thickening and stabilization model. *Tectonophysics*, *746*, 562–571.

Wang, H., van Hunen, J., Pearson, D. G., & Allen, M. B. (2014). Craton stability and longevity: The roles of composition-dependent rheology and buoyancy. *Earth and Planetary Science Letters*, *391*, 224–233.

Yoshida, M. (2010). Preliminary three-dimensional model of mantle convection with deformable, mobile continental lithosphere. *Earth and Planetary Science Letters*, *295*(1), 205–218.

Yoshida, M. (2012). Dynamic role of the rheological contrast between cratonic and oceanic lithospheres in the longevity of cratonic lithosphere: A three-dimensional numerical study. *Tectonophysics*, *532*, 156–166.

Yoshida, M., & Yoshizawa, K. (2021). Continental drift with deep cratonic roots. *Annual Review of Earth and Planetary Sciences*, *49*, 117–139.

Zhong, S. (2001). Role of ocean-continent contrast and continental keels on plate motion, net rotation of lithosphere, and the geoid. *Journal of Geophysical Research: Solid Earth*, *106*(B1), 703–712.

Zhong, S., Zuber, M., Moresi, L. N., & Gurnis, M. (2000). Role of temperature-dependent viscosity and surface plates in spherical shell models of mantle convection. *Journal of Geophysical Research: Solid Earth*, *105*(B5), 11063–11082.